Understanding the impact of C$_{60}$ at the interface of perovskite solar cells via drift-diffusion modeling

Timofey Golubev ✉ iD ; Dianyi Liu; Richard Lunt; Phillip Duxbury

Check for updates

View Online

Export Citation

Understanding the impact of C$_{60}$ at the interface of perovskite solar cells via drift-diffusion modeling

View Online   Export Citation   CrossMark

Timofey Golubev,[1,a] [iD] Dianyi Liu,[2] Richard Lunt,[1,2] and Phillip Duxbury[1]

AFFILIATIONS

[1] Department of Physics and Astronomy, Michigan State University, East Lansing, Michigan 48824, USA
[2] Department of Chemical Engineering and Materials Science, Michigan State University, East Lansing, Michigan 48824, USA

[a] Corresponding Author: golubevt@msu.edu

ABSTRACT

Perovskite solar cells have recently seen rapid improvements in performance with certified efficiencies of above 23%. Fullerene compounds are a very popular electron-transfer material in these devices. In a previous report, it has been shown that while an ultrathin fullerene layer of just 1 nm is sufficient to achieve good device performance, removal of this layer causes a drastic decrease in performance. We provide an explanation to these observed effects by use of a numerical device model. This work provides theoretical support to the experimental understanding of the dominant role of fullerenes in perovskite solar cells.

I. INTRODUCTION

Thin-film photovoltaics based on hybrid halide perovskites have attracted great interest in recent years[1-5] due to lower material and production costs than single-crystal devices as well as rapid improvements in perovskite device efficiencies to above 23%.[6] A typical planar heterojunction perovskite solar cell is composed of a perovskite absorber layer sandwiched between an electron transport layer (ETL) and a hole transport layer (HTL). The perovskite layer absorbs light which results in the photogeneration of free electrons and holes. The charge carriers will diffuse from higher to lower concentration and also drift due to the built-in electric field in the device. Electrons will on average move towards the ETL and holes towards the HTL. The main role of the ETL and HTL are to transport the respective carriers to the electrodes while blocking the opposite carrier type. For example, holes are unlikely to pass into the ETL and electrons are unlikely to pass into the HTL due to energy barriers. Both radiative and non-radiative recombination of carriers results in decrease in device performance. Radiative recombination is the annihilation of an electron from the conduction band with a hole in the valence band which results in the emission of a photon.

Non-radiative recombination, also known as trap-assisted recombination, occurs through a defect or trap which is an energy level in the band-gap. The trap can capture either an electron or hole (depending on the trap's energy level) which can recombine with a hole in the valence band or an electron in the conduction band respectively.

There is increasing interest in the application of fullerene compounds to perovskite photovoltaics.[7,8] Recently, Liu et. al.[9] observed that an ultrathin fullerene (C$_{60}$) layer can have a drastic impact on the performance of planar perovskite solar cells. Through a combination of fluorescence microscopy and impedance spectroscopy they showed that the main role of the C$_{60}$ is to efficiently extract electrons from the perovskite film. They demonstrated that even an ultrathin vapor deposited 1 nm C$_{60}$ layer works efficiently in the devices, while devices without C$_{60}$ exhibit poor performance.

The device architecture is as follows. The cells use poly(3,4-ethylenedioxythiophene):poly(styre-nesulfonic acid) (PEDOT:PSS) for the hole transport layer and bathocuproine (BCP) for the electron transport layer. The devices have a 1 nm, 20 nm, or no C$_{60}$ layer between the perovskite and BCP layers. All devices have a 80 nm Ag cathode and 100 nm indium-tin oxide (ITO) anode.
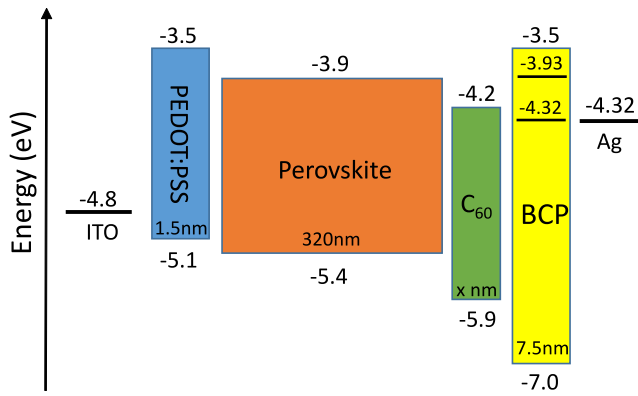
23 May 2025 06:28:45

FIG. 1. Energy levels and thicknesses of the device layers with the rectangles representing the bandgap of the material. The levels were found from a combination of literature values and fitting of the numerical model (Table I). The levels within the BCP bandgap are gap-states due to diffusion of Ag into BCP.

Fig. 1 shows the interior layer thicknesses and electronic energy levels of the devices, with the rectangles representing the bandgap of the materials. The energy alignment allows electrons to flow from the perovskite to the cathode and holes to flow from perovskite to the anode. It has been reported that electrons travel through BCP via gap-states which are thought to be caused by diffusion of the Ag into the BCP layer.[10–12] The energy levels of the gap-states as predicted by our numerical model are shown within the BCP rectangle.

In this work, we provide an explanation to the observed effects of ultrathin C_{60} on device performance by use of a numerical device model. The differences in electron extraction with C_{60} layer thickness are modeled by a reduced effective carrier mobility in the C_{60} layer or at the perovskite/BCP interface (for the devices without C_{60}). Our numerical results support the conclusions of Liu et. al regarding the role of C_{60} as essential for efficient electron extraction. Based on fitting of the model to the experimental results, the reason for the differences in performance between the devices with and without C_{60} is mostly due to a much lower electron mobility at a perovskite/BCP interface than at a perovskite/C_{60} interface. These results help clarify the role of the C_{60} layer as part of the ETL in a perovskite solar cell.

II. NUMERICAL MODEL

To model these devices, we use a one dimensional (1D) drift-diffusion approach based on the model reported in Sherkar et al.[13] to self-consistently solve the Poisson, continuity, and drift-diffusion equations using Gummel iterations[14] together with Scharfetter-Gummel discretization.[15] The Poisson equation relates the electron and hole densities (n and p respectively) to the electric potential ψ

$$\frac{\partial^2}{\partial x^2}\psi(x) = \frac{q}{\epsilon(x)}[n(x) - p(x)] \qquad (1)$$

where q is the elementary charge and ϵ is the dielectric constant. The current density for electrons and holes (J_n and J_p respectively) is related to the net free carrier generation rate $U(x)$ by the continuity

equations

$$\frac{\partial J_n}{\partial x}(x) = -qU(x) \qquad \frac{\partial J_p}{\partial x}(x) = qU(x) \qquad (2)$$

The charge generation profile is shown in Fig. 2 and was determined from a transfer-matrix optical model.[16]

The current densities are also related to the electric potential and charge carrier densities through the drift-diffusion equations

$$J_n = -qn\mu_n\frac{\partial}{\partial x}\psi + q\mu_n V_t\frac{\partial}{\partial x}n \qquad J_p = qp\mu_p\frac{\partial}{\partial x}\psi - q\mu_p V_t\frac{\partial}{\partial x}p \qquad (3)$$

where $V_t = kT/q$ is the thermal voltage.

The device is discretized into a one dimensional mesh with grid size of 0.25 nm with the anode and cathode located at $x = 0$ and $x = L$ respectively. The boundary conditions on the electric potential are

$$V(L) - V(0) + V_{ext} = V_{bi}, \qquad (4)$$

where V_{ext} is the applied bias and V_{bi} is the built-in field which is defined by the difference between anode and cathode work functions. The boundary conditions for the carriers are

$$n(0) = N_c exp\left(-\frac{E_{gap} - \phi_a}{V_t}\right) \qquad \text{and} \qquad p(0) = N_c exp\left(-\frac{\phi_a}{V_t}\right), \qquad (5)$$

where N_c is the density of states of both the conduction and valence band, E_{gap} is the perovskite bandgap, and ϕ_a is the injection barrier at the anode. Similarly, for the cathode

$$n(L) = N_c exp\left(-\frac{\phi_c}{V_t}\right) \qquad \text{and} \qquad p(L) = N_c exp\left(-\frac{E_{gap} - \phi_c}{V_t}\right), \qquad (6)$$

where ϕ_c is the injection barrier at the cathode.

We include both radiative and non-radiative (trap-assisted) carrier recombination. Radiative recombination is modeled by Langevin bimolecular recombination with the recombination rate given by
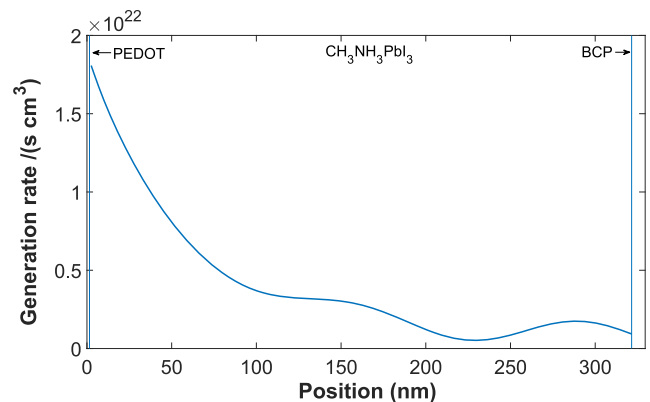
$$R_b = k_b(np - n_i^2), \qquad (7)$$

FIG. 2. Carrier photogeneration rate profile for the device without C_{60} as determined from the transfer-matrix optical model using the sum over wavelengths 350-750 nm. Position is displayed relative to the beginning of the HTL (PEDOT:PSS) layer.

TABLE I. Complete set of parameters used for the model. References for parameters obtained from literature are listed.

Parameter	Value	Source
Anode (ITO) work function	-4.8 eV	Ref. 18
HTL (PEDOT) HOMO Level	-5.1 eV	Ref. 19
HTL (PEDOT) LUMO Level	-3.5 eV	Ref. 19
Perovskite conduction band minimum	-3.9 eV	Ref. 13, 18, and 19
Perovskite valence band maximum	-5.4 eV	Ref. 13, 18, and 19
ETL (C_{60}) HOMO level	-5.9 eV	Fit
ETL (C_{60}) LUMO level	-4.2 eV	Fit
BCP gap-state levels	-3.93 eV, -4.32 eV	Fit/Ref. 10–12
BCP HOMO	-7.0 eV	Ref. 20
Cathode (Ag) work function	-4.32 eV	Ref. 20/Fit
Density of states (DOS)	8.1×10^{24} m^{-3}	Ref. 13
Perovskite relative permittivity	24.1	Ref. 13
PEDOT:PSS relative permittivity	3.0	Ref. 13
C_{60} relative permittivity	4.25	Ref. 21
BCP relative permittivity	4.25	Fit
Carrier mobility in perovskite	10^{-4} m^{2}V^{-1}s^{-1}	Ref. 22/Fit
Carrier mobility in PEDOT:PSS	4.5×10^{-6} m^{2}V^{-1}s^{-1}	Ref23
Carrier mobility in 20 nm C_{60}	1.6×10^{-4} m^{2}V^{-1}s^{-1}	Ref. 19
Hole mobility in 1 nm C_{60}	1.6×10^{-4} m^{2}V^{-1}s^{-1}	Ref. 19
Electron mobility in 1 nm C_{60}	1.6×10^{-5} m^{2}V^{-1}s^{-1}	Fit
Carrier mobility in BCP bulk	2×10^{-9} m^{2}V^{-1}s^{-1}	Fit
Electron mobility at perovskite/BCP interface	5×10^{-13} m^{2}V^{-1}s^{-1}	Fit
Maximum charge generation rate	1.97×10^{28} m^{-3}s^{-1}	Fit
Electron and hole capture coefficients	10^{-13} m^3 s^{-1}	Ref. 13
Bimolecular recombination constant	6×10^{-17} m^3 s^{-1}	Ref. 13
HTL/perovskite interface trap density	5×10^{21} m^{-3}	Ref. 13
Perovskite/ETL interface trap density	6×10^{20} m^{-3}	Ref. 13/Fit
PEDOT:PSS thickness	1.5 nm	Ref. 9
Perovskite thickness	320 nm	Ref. 9
BCP thickness	7.5 nm	Ref. 9
Grid spacing	0.25 nm	

where k_b is the bimolecular recombination constant and n_i is the intrinsic carrier density. Bimolecular recombination is assumed to occur only in the perovskite layer. It is not considered in the transport layers because of the very low density of minority carriers in those layers which makes the recombination rate many orders of magnitude less than in the perovskite. Non-radiative trap assisted recombination is assumed to occur only in 5 nm thick regions inside the perovskite layer near the HTL and ETL interfaces and is described by the Shockley-Read-Hall equation

$$R_{SRH} = \frac{C_n C_p N_{trap}(np - n_1 p_1)}{C_n(n + n_1) + C_p(p + p_1)}, \tag{8}$$

where C_n and C_p are electron and hole capture coefficients and

$$n_1 = N_{LUMO} exp\left(-\frac{E_{LUMO} - E_t}{k_B T}\right)$$

and

$$p_1 = N_{HOMO} exp\left(-\frac{E_t - E_{HOMO}}{k_B T}\right). \tag{9}$$

The trap energies E_t are assumed to be located in the middle of the bandgap since this energy gives most effective recombination.[17] As in Sherkar et. al., the traps are assumed to have neutral charge. Ions are not considered since there is no experimental evidence that ions are a key factor affecting the physics of these devices. For example, there is no hysteresis in the JV curves of devices with C_{60}, therefore the hysteresis observed in the 0nm C_{60} devices are likely due to space charge effects rather than ions.[9]

Table I provides the complete set of parameters used for the model with references for parameters taken from literature listed.[9–13,18–23] Less efficient electron transport at the perovskite/BCP interface is modeled by a decreased electron mobility value in a 0.5 nm interface region. For the 1 nm C_{60}, less efficient electron transport due to incomplete coverage of C_{60} is modeled by a reduced effective mobility for C_{60}.

III. RESULTS AND DISCUSSION

We find a good agreement between the experimentally measured and numerically predicted current-voltage (JV) curves (Fig. 3).
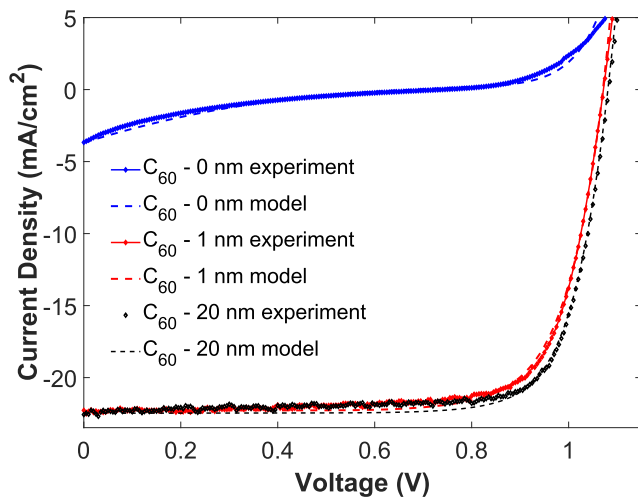
FIG. 3. Comparison of the JV curve results from the experiment and numerical model.

We see that the C_{60} layer is essential for good device performance and that a 1 nm C_{60} layer is sufficient for good performance, with only a small improvement achieved when the layer thickness is increased to 20 nm. The fit to experiment suggests that the electron mobility at a perovskite/C_{60} interface is significantly higher than at a perovskite/BCP interface (case of no C_{60}). This higher mobility models a more efficient extraction of electrons from the perovskite to the ETL.

To determine the reason for the experimentally observed performance loss in the 0 nm C_{60} devices, the influence of electron mobility and traps at the perovskite/BCP interface was computationally studied (Fig. 4). For the mobility trials, we set all parameters as in Table I and only vary the perovskite interface mobility. For testing the effects of the interface trap density, we first raise the perovskite interface mobility to the same value as in the device with 20 nm C_{60} (2×10^{-9} m²/Vs) to remove the effect of lower mobility, and then vary the trap density. We find that mobility mostly influences the short-circuit current, while trap density mostly influences the open-circuit voltage and fill factor. Fig. 4a shows how a decrease in perovskite interface mobility significantly affects the short-circuit

current and fill factor of the device. For the devices without a C_{60} layer, fitting the model to the experimental results suggests an electron mobility of 5×10^{-13} m²/Vs. An increased trap density at the interface (Fig. 4b) does not result in the drastic short-circuit current loss which is experimentally observed; therefore the dominant factor is a low interface mobility.

These results support the fluorescence microscopy experiments of Liu et al. which showed that while adding thin C_{60} layers to perovskite cause a significant decrease in photoluminescence (PL), placing BCP alone onto perovskite does not significantly change the PL efficiency (neat perovskite films are as bright or brighter with BCP).[9] A quenched PL intensity indicates a smaller accumulation of electrons. If the improvement in performance due to C_{60} was due to small molecules passivating defect states, we would expect the PL quenching with BCP to be similar to that of C_{60}. Since this is not the case, it was concluded that C_{60} acts to greatly improve the efficiency of electron extraction from perovskite. Similar results were reported in the literature for perovskite devices using TiO_2 as the ETL; addition of fullerene compounds to the ETL enhanced electron extraction at the perovskite/ETL interface.[24,25]

We gain more insight into the space-charge effects in these devices by considering the charge density profiles for devices with different C_{60} thicknesses at zero applied bias (Fig. 5). In the 0 nm C_{60} device, due to the low mobility at the perovskite/BCP interface the electron extraction is poor and results in a lower extraction of electrons than holes from the device as seen from the low electron density in the BCP layer at the right side of Fig. 5. This can also be understood as an imbalance in mobilities of the majority charge carrier through their corresponding transport layer or equivalently as the addition of an extraction barrier for electrons. A charge accumulation at the perovskite/BCP interface occurs. In contrast, the devices with C_{60} have no electron accumulation within the perovskite layer. This supports the fluorescence microscopy measurements done on these devices which show a much stronger photoluminescence, indicating a larger electron accumulation for the devices without C_{60} than with C_{60}.[9] In the devices with C_{60}, due to the efficient electron extraction from the perovskite, there is a high electron density in the C_{60} together with a very low hole density and an injection barrier which prevents electrons from moving back into the perovskite. The high electron transfer efficiency also reduces the loss of free carriers due to carrier recombination within the perovskite layer. This means that more electrons can be
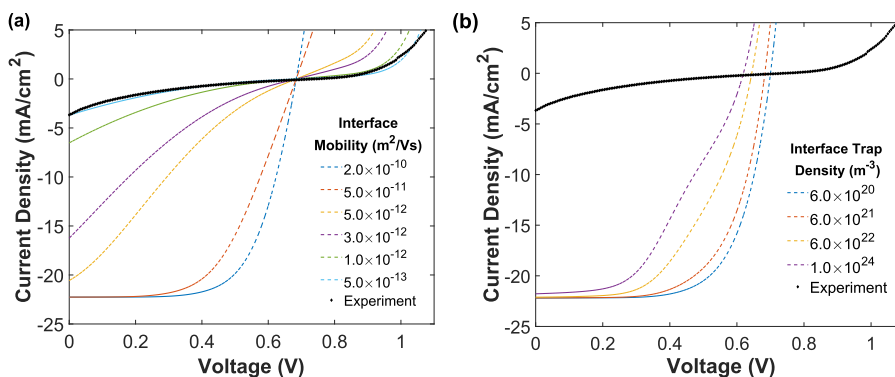

FIG. 4. JV curves showing the effects of perovskite/BCP interface carrier mobility (a) with ETL trap density set to 6×10^{20} m⁻³ and trap density (b) on the 0 nm device with perovskite/BCP interface mobility set to 2×10^{-9} m²/Vs (the same value as for the 20 nm C_{60} device). All other parameters are kept the same as in Table I.
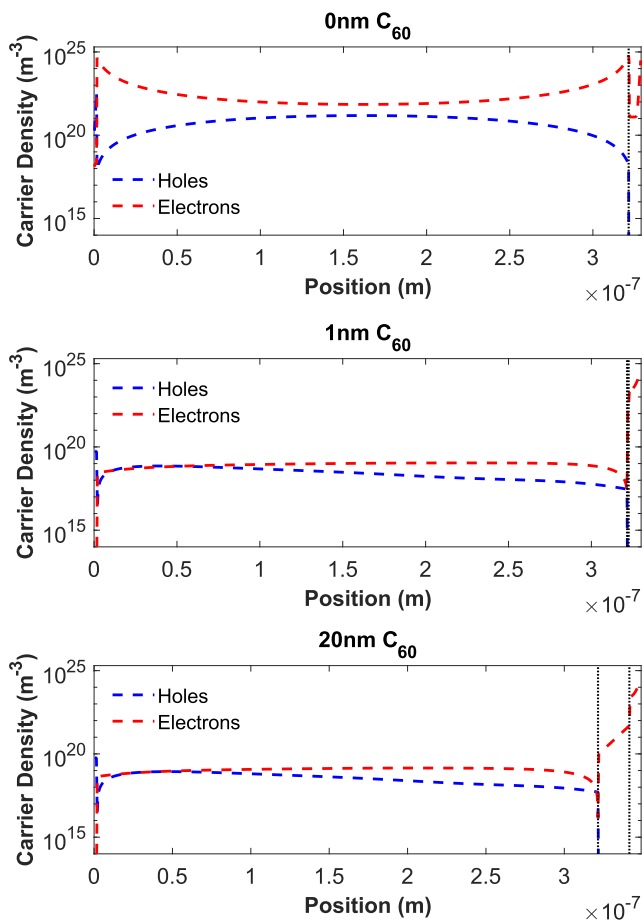
FIG. 5. Charge carrier densities for the simulated devices with 0 nm, 1 nm, and 20 nm C_{60} under illumination at zero applied bias. The perovskite/C_{60} and C_{60}/BCP interfaces are marked by dotted black lines. The parameters used are listed in Table I.

Schottky barrier.[26] The charge transport through this barrier could be a tunneling process which is exponentially related to the height of the barrier. However, using an energetic barrier at the perovskite/BCP interface instead of a low interface effective mobility does not reproduce the experimental results (see supplementary material S1). A more likely reason for the less efficient transport could be related to a difference between the two interfaces at the molecular level causing the perovskite/C_{60} interface to have a better electron transport pathway.

Next we offer an explanation for the origin of the S-shaped JV curve observed in the 0 nm C_{60} device (Fig. 3). Several groups have proposed explanations for the appearance of S-shaped JV curves in solar cells. They have been attributed to various factors including interface dipoles,[27] charge accumulation,[20,28] injection or extraction barriers,[29] imbalanced mobilities,[30] and poor extraction of electrons near the cathode due to a mobility drop-off.[31] In the device studied here the origin is likely a combination of several of the above, namely an injection barrier, mobility drop-off (equivalently imbalanced mobilities), charge accumulation, and interfacial dipole.

Fig. 6 shows the 0 nm C_{60} device under 0.7 V and 0.9 V applied bias which correspond respectively to points before and after the onset of forward current in the device. At 0.7 V, we see that there is no longer a dip in electron density within the BCP which indicates that electrons are being injected from the cathode into BCP. However, the electrons are not being injected into the perovskite layer as seen by the steep difference in electron density on opposite sides of the perovskite/BCP interface. The electron accumulation in BCP is caused by a combination of the 0.42 eV injection barrier for electrons (see Fig. 1) and the low electron mobility at the perovskite/BCP interface which prevents efficient injection into the perovskite layer. The injection barrier and low interface electron mobility prevent an injection current from flowing. As we further increase the applied voltage from 0.7 V, there is an even larger accumulation of electrons within the BCP near the perovskite/BCP interface and now also an accumulation of holes on the other side of the interface, forming a dipole. The dipole effectively decreases the injection barrier for electrons, however as long as there still remains an injection barrier, no injection current will flow. Therefore, the net current in the device is near zero until the applied voltage is sufficient to overcome the injection barrier (i.e. about 0.9 V). Notice that the width of the flatter region in the JV curve increases with decreasing interface mobility (Fig. 4a) since a

extracted to the BCP than in the 0 nm C_{60} device, resulting in a higher current.

A possible reason for the reduction of mobility at the perovskite/BCP interface could be the formation of a back-to-back
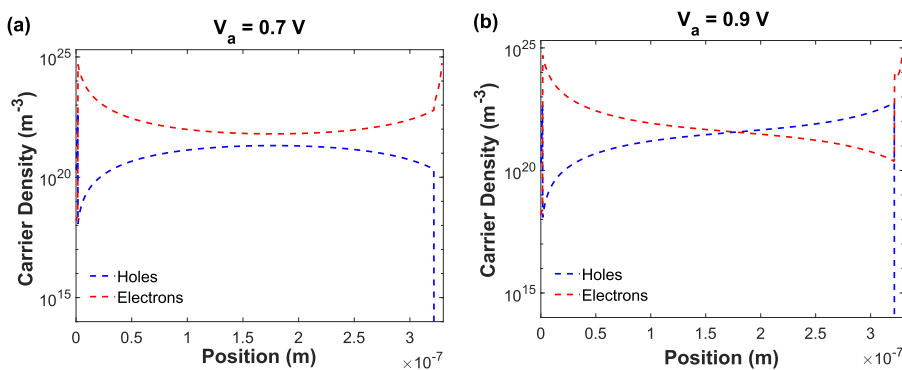

FIG. 6. Charge carrier densities for device with 0 nm C_{60} under illumination at 0.7 V (a) and 0.9 V (b) applied bias. The parameters used are listed in Table I.

lower interface mobility requires a stronger net field (and thus a higher applied voltage) to establish an injection current across the interface.

IV. CONCLUSION

A 1D drift-diffusion model for planar perovskite solar cells has been used to describe recent experimental results for inverted planar structure perovskite devices which use fullerene layers for electron transport. By systematically studying the effects of interface mobility and trap density on the JV curves, we find that poor electron extraction at the perovskite interface modeled by a decreased carrier mobility is the main cause of the severe decrease in device performance when there is no C_{60} layer. We demonstrate that the decrease in performance is not due to an increased trap density at the interface. We have also analyzed and provided an explanation for the S-shaped JV curve of the 0 nm C_{60} device. The main origin of the S-shape is likely due to the non-equal mobilities in the HTL and ETL which results in charge accumulation and the formation of an interface dipole. Our results support the conclusion that very little C_{60} is needed to enhance carrier extraction. Ultimately, this work helps clarify the role of fullerenes in perovskite solar cells.

SUPPLEMENTARY MATERIAL

See supplementary material for results showing use of an energetic barrier at the perovskite/BCP interface and the effects of varying the HOMO/LUMO levels of the HTL/ETL in the 0 nm C_{60} device.

REFERENCES

[1] M. A. Green, A. Ho-Baillie, and H. J. Snaith, Nature Photonics **8**, 506 (2014).

[2] H. J. Snaith, The Journal of Physical Chemistry Letters **4**, 3623 (2013).

[3] N.-G. Park, Materials Today **18**, 65 (2015).

[4] Z. Li, T. R. Klein, D. H. Kim, M. Yang, J. J. Berry, M. F. A. M. van Hest, and K. Zhu, Nature Reviews Materials **3**, 18017 (2018).

[5] Z. Shi and A. Jayatissa, Materials **11**, 729 (2018).

[6] Nrel best research-cell efficiencies, https://www.nrel.gov/pv/assets/pdfs/pv-efficiencies-07-17-2018.pdf, accessed: 2018-10-12.

[7] Y. Fang, C. Bi, D. Wang, and J. Huang, ACS Energy Letters **2**, 782 (2017).

[8] E. Castro, J. Murillo, O. Fernandez-Delgado, and L. Echegoyen, Journal of Materials Chemistry C **6**, 2635 (2018).

[9] D. Liu, Q. Wang, C. J. Traverse, C. Yang, M. Young, P. S. Kuttipillai, S. Y. Lunt, T. W. Hamann, and R. R. Lunt, ACS Nano **12**, 876 (2018).

[10] T. Sakurai, S. Toyoshima, H. Kitazume, S. Masuda, H. Kato, and K. Akimoto, Journal of Applied Physics **107**, 043707 (2010).

[11] H. Yoshida, The Journal of Physical Chemistry C **119**, 24459 (2015).

[12] J. Lee, S. Park, Y. Lee, H. Kim, D. Shin, J. Jeong, K. Jeong, S. W. Cho, H. Lee, and Y. Yi, Phys. Chem. Chem. Phys. **18**, 5444 (2016).

[13] T. S. Sherkar, C. Momblona, L. Gil-Escrig, H. J. Bolink, and L. J. A. Koster, Adv. Energy Mater. **7**, 1602432 (2017).

[14] H. Gummel, IEEE Trans Electron Devices **11**, 455 (1964).

[15] D. Scharfetter and H. Gummel, IEEE Trans Electron Devices **16**, 64 (1969).

[16] G. F. Burkhard, E. T. Hoke, and M. D. McGehee, Adv. Mater. **22**, 3293 (2010).

[17] J. G. Simmons and G. W. Taylor, Phys Rev B **4**, 502 (1971).

[18] O. Malinkiewicz, A. Yella, Y. H. Lee, G. M. Espallargas, M. Graetzel, M. K. Nazeeruddin, and H. J. Bolink, Nat. Photon. **8**, 128 (2013).

[19] P.-W. Liang, C.-C. Chueh, S. T. Williams, and A. K.-Y. Jen, Adv. Energy Mater. **5**, 1402321 (2015).

[20] C. Chen, S. Zhang, S. Wu, W. Zhang, H. Zhu, Z. Xiong, Y. Zhang, and W. Chen, RSC Advances **7**, 35819 (2017).

[21] Ses research: Properties of carbon 60, https://www.sesres.com/physical-properties/, accessed: 2018-03-07.

[22] L. M. Herz, ACS Energy Letters **2**, 1539 (2017).

[23] Q. Wei, M. Mukaida, Y. Naitoh, and T. Ishida, Adv. Mater. **25**, 2831 (2013).

[24] K. Wojciechowski, S. D. Stranks, A. Abate, G. Sadoughi, A. Sadhanala, N. Kopidakis, G. Rumbles, C.-Z. Li, R. H. Friend, A. K.-Y. Jen, and H. J. Snaith, ACS Nano **8**, 12701 (2014).

[25] C. Tao, S. Neutzner, L. Colella, S. Marras, A. R. S. Kandada, M. Gandini, M. D. Bastiani, G. Pace, L. Manna, M. Caironi, C. Bertarelli, and A. Petrozza, Energy & Environmental Science **8**, 2365 (2015).

[26] G. Horowitz, Adv. Funct. Mater. **13**, 53 (2003).

[27] A. Kumar, S. Sista, and Y. Yang, J. Appl. Phys. **105**, 094512 (2009).

[28] J. Wang, X. Ren, S. Shi, C. Leung, and P. K. Chan, Org. Electron. **12**, 880 (2011).

[29] W. Tress, K. Leo, and M. Riede, Adv. Funct. Mater. **21**, 2140 (2011).

[30] W. Tress, A. Petrich, M. Hummert, M. Hein, K. Leo, and M. Riede, Appl. Phys. Lett. **98**, 063301 (2011).

[31] B. Y. Finck and B. J. Schwartz, Appl. Phys. Lett. **103**, 053306 (2013).

23 May 2025 06:28:45